Aging Pathobiology and Therapeutics 2021; 3(4):107-126 ***107***
DOI: 10.31491/APT.2021.12.074

PathoClock and PhysioClock in mice recapitulate human multimorbidity and heterogeneous aging

Shabnam Salimi[a,*], Christina Pettan-Brewer[b], Warren Ladiges[b,*]

[a] *Department of Epidemiology and Public Health, University of Maryland Baltimore, School of Medicine, Baltimore, MD, USA.*
[b] *Department of Comparative Medicine, School of Medicine, University of Washington, Seattle, WA 98195, USA.*

Abstract

Background: Multimorbidity is a public health concern and an essential component of aging and healthspan but understudied because investigative tools are lacking that can be translatable to capture similarities and differences of the aging process across species and variability between individuals and individual organs.
Methods: To help address this need, body organ disease number (BODN) borrowed from human studies was applied to C57BL/6 (B6) and CB6F1 mouse strains at 8, 16, 24, and 32 months of age, as a measure of systems morbidity based on pathology lesions to develop a mouse PathoClock resembling clinically-based Body Clock in humans, using Bayesian inference. A mouse PhysioClock was also developed based on measures of physiological domains including cardiovascular, neuromuscular, and cognitive function in the same two mouse strains so that alignment with BODN was predictable.
Results: Between- and within-age variabilities in PathoClock and PhysioClock, as well as between-strain variabilities. Both PathoClock and PhysioClock correlated with chronological age more strongly in CB6F1 than C57BL/6. Prediction models were then developed, designated as PathoAge and PhysioAge, using regression models of pathology and physiology measures on chronological age. PathoAge better predicted chronological age than PhysioAge as the predicted chronological and observed chronological age for PhysioAge were complex rather than linear.
Conclusion: PathoClock and PhathoAge can be used to capture biological changes that predict BODN, a metric developed in humans, and compare multimorbidity across species. These mouse clocks are potential translational tools that could be used in aging intervention studies.
Keywords: Multimorbidity, aging, pathology, physiology, pathoClock, physioClock, pathoAge, physioAge

Introduction

An increase in the population of older adults comes with a rise in age-related health conditions [1]. With the increase in lifespan in the population, healthspan has become a focus of research and public health policies [2, 3]. Therefore, measurements of healthspan require cross-species translatable tools for preclinical and clinical studies [4-6]. For example, with distinct frailty indices in humans, mouse models of frailty have been developed [7-9]. Recent studies of age-related pathology using a geropathology platform that generates age-related lesion scores [10] have suggested a stronger correlation between age-related pathologies and chronological age than frailty indices [5, 10, 11].

A crucial aspect of healthspan is the burden of multimorbidity, conventionally described as having two or more diseases [2]. While comorbidity is commonly used to assess clinical disease burden in people, especially with increasing age, it has not been well characterized in animal models in a manner that has significant translational relevance.

* Corresponding author: Warren Ladiges
Mailing address: Department of Comparative Medicine, School of Medicine, University of Washington, Seattle, WA 98195, USA.
Email: wladiges@uw.edu
* Corresponding author: Shabnam Salimi
Mailing address: Department of Epidemiology and Public Health, University of Maryland Baltimore, School of Medicine, Baltimore, MD, USA.
Email: shabnam.salimi.m.d@gmail.com
Received: 19 October 2021 / Accepted: 23 December 2021

Studies of rodent models have extensively focused on lifespan, using either chronological age or time to death as outcomes [12-14]. In recent years, healthspan has become an increasingly important focus of research with an increase in the older population [11, 15]. Multimorbidity is one of the crucial aspects of healthspan [4], but the study of multimorbidity in mammalian models has been limited. Most studies have used a frailty index (FI) of one kind or another as a translatable tool to report health in humans or mice. Previously, FIs were adapted to apply to C57BL/6 mice [8], and a study of C57BL/6 showed that FI scores were related to heart hypertrophy [9]. However, the disease status of organs with morbidity and the histopathological changes associated with specific organs were not studied. In addition, whether the physiological changes tracked with end-point pathologies was not reported.

Moreover, human FIs usually incorporate the disability state into the score, skewing the measures toward those with a disability rather than predicting disability as one possible deteriorating outcome prior to mortality [7].

One approach to better define comorbidity in animal models is to consider the presence of pathology at the organ level. While many studies have focused on how aging and age-related diseases affect individual organs, each organ's contribution to overall aging has been overlooked. A recent study of multimorbidity in the human population has suggested body organ disease number (BODN) as an index of multimorbidity [16]. The disease levels of each organ are heterogeneously incorporated into BODN at the individual level. The integrated burden of disease incorporated into BODN for an individual has been shown to outperform chronological age to predict BODN and has been termed Body Clock [16].

Therefore, it is speculated that an organ-based pathology system in aging mice, such as the recently developed geropathology grading platform [10] could be used to define a measurable phenotype designated as PathoClock. By applying the Bayesian inference [9], the mouse-specific PathoClock could be a useful tool to simulate the human Body Clock. In addition, physiological and functional measurements are routinely determined in aging mouse studies. Therefore, this type of preclinical data could be used to predict heterogeneous BODN resulting in a mouse-specific PhysioClock.

Some studies of aging have used biological measures tied to chronological age as outcome to predict biological age [12]. The current manuscript introduces PathoAge and PhysioAge using Bayesian inference and regression models of pathology and physiology measures, respectively, to understand how pathology and physiology based on chronological age align with biological age.

Methods

Mice and study design

CB6F1 and C57BL/6 male mice were obtained from the National Institute on Aging (NIA) aged rodent facility (Charles River @ Laboratories) and housed in a specific pathogen-free facility at the University of Washington (UW) School of Medicine. Standard care procedures were followed including rodent chow, reverse osmosis purified automatic watering, 12: 12 light cycle, and 72 ± 2 degrees F room temperature. All animal protocols were approved by the UW Institutional Animal Care and Use Committee. Animals were euthanized for pathology studies at ages 8, 16, 24, and 32 months, three months after the physiological domains were measured.

Physiological assessment

(1) Cardiac function. Echocardiography was used to assess systolic and diastolic function in mice. The Siemens Acuson CV-70 system using standard imaging planes: M-mode, conventional, and Tissue Doppler imaging, was used to measure cardiac function, including the ratio of the aorta and left atrium (AO/LA ratio), ejection time (ET msec), isovolumic contractile time (IVCT msec), isovolumic relaxation time (IVRT msec). The E/A ratio as a marker of the left ventricle function indicates the peak velocity blood flow from left ventricular relaxation in early diastole (the E wave) to peak velocity flow in late diastole caused by atrial contraction (the A wave). Myocardial performance index (MPI) incorporates both systolic and diastolic time intervals in expressing a global systolic and diastolic ventricular function quantified as MPI = (IVCT + IVRT)/ET [17]. The methods are described elsewhere [18].

Neuromuscular Function. Established tests of muscular activity were used to assess changes in muscle strength and coordination with age. Several assessments including coordinated walking ability, grip strength, novel environment response, and self-motivated running, were used to address variability due to motivation, emotionality, or sensory deficits.

(2) Coordinated walking ability. Coordinated walking ability was assessed using a rotarod apparatus (Rotamax 4/8, Columbus Instruments, Inc.) that tested the ability of the mouse to maintain walking speeds on a rotating rod. Mice were placed in the lanes of the rotarod with the initial rod speed set at 0 RPM. The speed was progressively increased by 0.1 RPM/sec (0 to 40 RPM over 5 minutes) until all mice had been dislodged as determined by an infrared sensor. The time in seconds was recorded. Three successive runs were performed per day for three days. Therefore, there is an evaluation of motor function and performance learning. The assay was performed by the same person, at the same location. Data are reported as the median of 3 trials and standardized by body weight.

(3) Grip strength. Forelimb grip strength was analyzed using a force tension apparatus (San Diego Instruments Columbus Instruments, Inc.). Prior to the test, each mouse was weighed to the nearest 0.1 g. Once mice gripped the stationary bar with their forepaws, they were stretched horizontally while held at the base of their tails. Mice were pulled gradually until they let go of the bar. The process was repeated 5 times to determine the peak grip force value (gram-force) standardized to body weight [19].

(4) Novel environment response. Mice were assessed for movement levels in a novel cage environment using an open field photobeam apparatus (Photo beam Activity System, Columbus Instruments, Inc.). Each mouse was placed for five minutes in a clear, rectangular, plastic container the size of a standard mouse cage, which had a rectangular grid of infra-red beams inside, three on the X-axis and four on the Y-axis to measure horizontal movement (lateral activity). Another grid set of beams were positioned above the lower set to measure vertical movement (rearing). Beam breaks were counted for activity and rearing and further classified for either the central or peripheral part of the box as a measure of anxiety. The activity was assessed for a five-minute period on three consecutive days [20].

(5) Self-motivated running. The self-motivated running distance was measured by a voluntary wheel running apparatus over three days as described by Goh and Ladiges (2015) [21]. Mice were placed into a standard cage with a slanted plastic saucer-shaped wheel (Med Associates, Inc.). Mice were acclimated to the cage for 48 hours with the wheel locked, after which the wheels were unlocked and the distance each mouse ran was tracked by a computer over 72 hours including both light and dark cycles. Total distance in kilometers was recorded.

(6) Cognitive Function. Cognition was assessed using the radial water tread (RWT) maze, an assay used to assess memory as previously described [22, 23]. The RWT detects changes in hippocampal function in mice. Briefly, mice are introduced into an approximately 30-inch circular galvanized enclosure with waste-deep water and peripheral escape holes in the sides at regular intervals, all closed except one which leads to a dark "safe box" with a heating pad. The inside walls contain spatial cues for the animal to find the escape route with repeated trials. The animals were given three trials per training day, and the testing period ran across successive days to test long-term memory acquisition. Performance was recorded by direct observation [24].

Various physiological domains described above were used to predict body organ disease number (BODN) and define a mouse-specific PhysioClock independent of chronological age.

Pathological assessments

Cataract assessment. The presence and severity of cataracts were assessed by slit-lamp ophthalmoscopy on unanesthetized mice after dilation with a 3: 1 volume mixture, respectively, of tropicamide and phenyl hydrochloride to achieve full dilation. The degree of lens opacity was rated by half steps from 0 (completely clear) to 4 (complete opacity of a mature cataract) as previously described [25].

Histopathology assessment. Histopathology assessments were performed on Hematoxylin and Eosin-stained 4-micron tissue sections from heart, kidney, liver, pancreas, muscle, lung, and brain as previously described [10]. Age-related lesion severity levels were determined by a scoring system from 0 (no lesion present) to a range of 1 to 4 (lesion presence and severity). The absence or presence and severity of age-related lesions were then used to determine organ morbidity defined as the presence of two-level 1 lesions or one lesion with a score of 2 or greater. The body organ disease number (BODN) was then calculated as the number of organ systems with morbidity as a proxy of multimorbidity and a counterpart of clinically determined BODN in humans. With the premise that different pathology entity levels incorporate into BODN heterogeneously, all organ pathologies in a model were used to predict BODN for each mouse to quantify PathoClock independent of chronological age.

Statistical analyses

BODN was considered an ordinal outcome as a number of organ systems with at least two positive pathology criteria at level 1 or at least one pathology at level 2 or more. We recorded the levels starting from 1 as an ordinal value. Bayesian inference was used for ordinal outcome [26] also ordinal [27], binary, or continuous predictors depending on the type of predictor variables [27-30]. Bayesian inference approach was used comprising two components: 1) Prior knowledge on the estimates (parameters), as the information before observing the data $P(\Theta)$ where Θ indicates the parameters; and 2) the likelihood $P(Y|\Theta)$ of the information contained in the data (Y). Using the Bayes formula, the posterior distribution of the parameters $P(\Theta|Y)$ was obtained, which can be updated when encountering new data [28].

Applying the conditional probability given the known data on BODN, the Bayesian inference framework yields the posterior density of beta estimate coefficients and 95% credible interval (CI) that each pathology level incorporates into BODN, or each physiological measure predicts BODN. For each coefficient parameter, we determined the distributions of their prior parameters using weak priors [28]. For the classes of beta coefficients and intercept, the prior estimate with a normal distribution (mean: $\mu = 0$, variance $\sigma = 10$), and for the class standard deviation (sd) which indicated the variation of levels related to varying age, the half-Cauchy (0,10) was used. The uniform prior with a Dirichlet distribution was used for ordinal predictors [i.e., (2, 2) for $\zeta 1$ and $\zeta 2$ (simplex parameters) for a three-level pathology predictor]. We reported the standard deviation for the model level in multilevel analyses (sd), and sigma which is the variance of a continuous outcome in the model with a gaussian family [27, 30]. Posterior predict function was then used in the Bayesian framework [28, 30] to predict individual-based BODN for each mouse using all organ pathology levels, termed PathoClock. The correlation of PathoClock and chronological age was quantified as a rate of pathology-based biological age.

The model accuracy was assessed with Leave-One-Out Cross-Validation (LOO-CV) ($k < 0.7$) which with a Pareto-smoothed importance sampling diagnostic $k < 0.7$ indicating the LOO-CV computation is reliable and there

are no outlier observations. Also, a Bayesian inference approach called "stacking" determines model weights for each model to predict an outcome [29, 31]. The Leave-One-Out R squared (LOO_R2) was used to determine the R2 of the model to show how a model explains the outcome [32].

All statistical analyses were performed using the Bayesian "brms" software package [30]. A dynamic Hamiltonian Markov chain Monte Carlo (MCMC) algorithm [30, 33] was used to obtain posterior draws using a minimum of six chains and a minimum of 10,000 iterations. Model averaging was then used in the Bayesian framework, called stacking, which provides weight for the best model predicting BODN [34]. For pathologies of more than two levels, we used the "monotonic" effect implemented in the Bayesian inference framework which defines the probability of coefficient estimates with Dirichlet distribution [27]. The physiological measures like grip strength or rotarod, which have an inverse association with BODN, were transformed so that were multiplied by -1 to develop PhysioClock.

Commonly, studies statistically have regressed biomarkers or phenotype measurements on chronological age to assess how they predict chronological age [12]. In concert with such an approach, we developed PhysioAge and PathoAge, regressing the allocated physiological measures and pathological level measurements, respectively, on chronological age using a gamma distribution. In CB6F1, to develop PhysioAge, we included normalized grip strength, rotarod test at day 3, open field activity at day3, open field rearing at day 2, distance, AO/LA ratio, ET (ejection time), LVM, MPI, and Maze test at day 5. In C57BL/6, for PhysioAge we included nine physiologic measures including AO, LA, natural log-transformed E/A ratio, LVMI and MPI, Maze test at day 5, open field activity at day 1, rotarod at day 2, and normalized grip strength.

Results

Physiological performance predicts body organ disease number

Cardiac function. Echocardiography was used to measure cardiac function. For CB6F1, the ratio of aortic valve diameter to left atrium dimension (AO/LA) was inversely associated with increase in BODN (beta = -2.3, 95% CI: -4.3 to -0.32), E to A waves ratio (beta = -1.5, 95% CI: -2.9 to -0.15), on natural logarithm scales and with relatively high uncertainty (wide credible interval CI) isovolumic contraction time (IVCT) [beta = 1.48, 95% CI: 0.02-3.0], left ventricular internal diameter end diastolic (LVIDd) [beta = 7.6, 95% CI: 0.13 = 15.0], left ventricular internal diameter end systolic (LVIDs) (beta = 4.7, 95% CI: 0.47-9.03), (considering both systolic and diastolic measures (MPI) [beta = 2.03, 95% CI = 0.11-4.01], ejection time (beta = - 6.6, 95% CI: -12.0 to -0.7) predicted BODN (Figure 1A, Table 1A). Chronological age per se was strongly associated with BODN (beta = 0.34, 95% CI = 0.24-0.46) while stacking of the cardiovascular models predicting BODN revealed cardiovascular physiologies predict BODN stronger than chronological age predicted BODN so that the model weight for chronological age turned to zero. The largest model weights were allocated to ejection time (ET: 27.5%), E/A ratio (26%), IVCT (21.5%), MPI (17%), AO/LA ratio (8%) that MPI by 46%, LVIDd by 19%, E/A ratio by 28.5%, IVCT (6%) with the rest also turned to zero.

For C57BL/6 mice, aortic valve diameter (beta = 2.3, 95% CI: 0.6-4.0), LA (beta = 1.65, 95% CI: 0.13-3.28), IVCT (beta = -1.79, 95% CI: -0.35 to -0.14), LVIDs (beta = 4.1, 95% CI: 0.69-7.8) were significantly predicted BODN. With wide uncertainty (credible interval including zero) both AO/LA ratio and E/A ratio were inversely predicted BODN.

Using model averaging overall physiological measures of the cardiovascular system in C57BL/6 showed that MPI by 72.6%, LVIDs by 22%, E/A ratio by 0.5%, aortic diameter (mm) by 1 %, and left atrial diameter (mm) by 4.5 % predicted BODN and were included in the final model as cardiovascular physiology domains to quantify PhysioClock.

Neuromuscular Function. Rotarod test for CB6F1 indicating disturbed balance state predicted increase in BODN measured at day 2 (beta = -1.7, 95% CI: -2.86 to -0.62). Stacking of the models showed that the model assessed balance state at day 2 weighed 75.4% to predict BODN compared to day 1 (17.1%) and day 3 (7.5%). Therefore, we included rotarod test day 2 in the PhysioClock model. The lower the grip strength, the larger the BODN was (beta = -5.9, 95% CI: -10.5 to -1.6), and it was more robust when normalized to body mass (beta = -7.3, 95% CI: -11.4 to -3.8). Comparing models showed that the normalized grip strength over body size was a stronger predictor of BODN at 98.3%.

For C57BL/6 mice, balance states at days 1 and 2 significantly predicted BODN with day -2 model weight (53.2%) larger than day 1 (46.8%). Therefore day 2 was included in the Physiology Clock. Like CB6F1, the grip strength in C57BL/6 normalized over body mass was a stronger predictor of BODN (Figure 1B, Table 1B). In this strain, only grip strength normalized by body mass significantly predicted BODN with credible intervals excluding zero. However, wide CI (beta = -3.2, 95% CI = -6.4 to -0.18) showed some degree of uncertainty.

Cognitive Function. For CB6F1 mice, time of learning maze measured at day 1, 2 ,3 and 4 was associated with increased in PathoClock (day 1: beta = 1.13, 95% CI = 0.18-2.07; day 2: beta = 0.87, 95% CI = 0.21-1.54; day 4: beta = 0.45, 95% CI = 0.11-0.78). The longer the learning process at day 1 the larger the PathoClock was. The longer maze test indicated poorer cognition and predicted larger PathoClock (day 5: beta = 0.49, 95% CI = 0.15-0.83; day 12: beta = 0.92, 95% CI: 0.49-1.38). Likewise, results were detected for observed BODN (day 2: beta = 1.5, 95% CI: 0.22-2.79; day 4: beta = 0.62, 95% CI: 00.08-1.18)

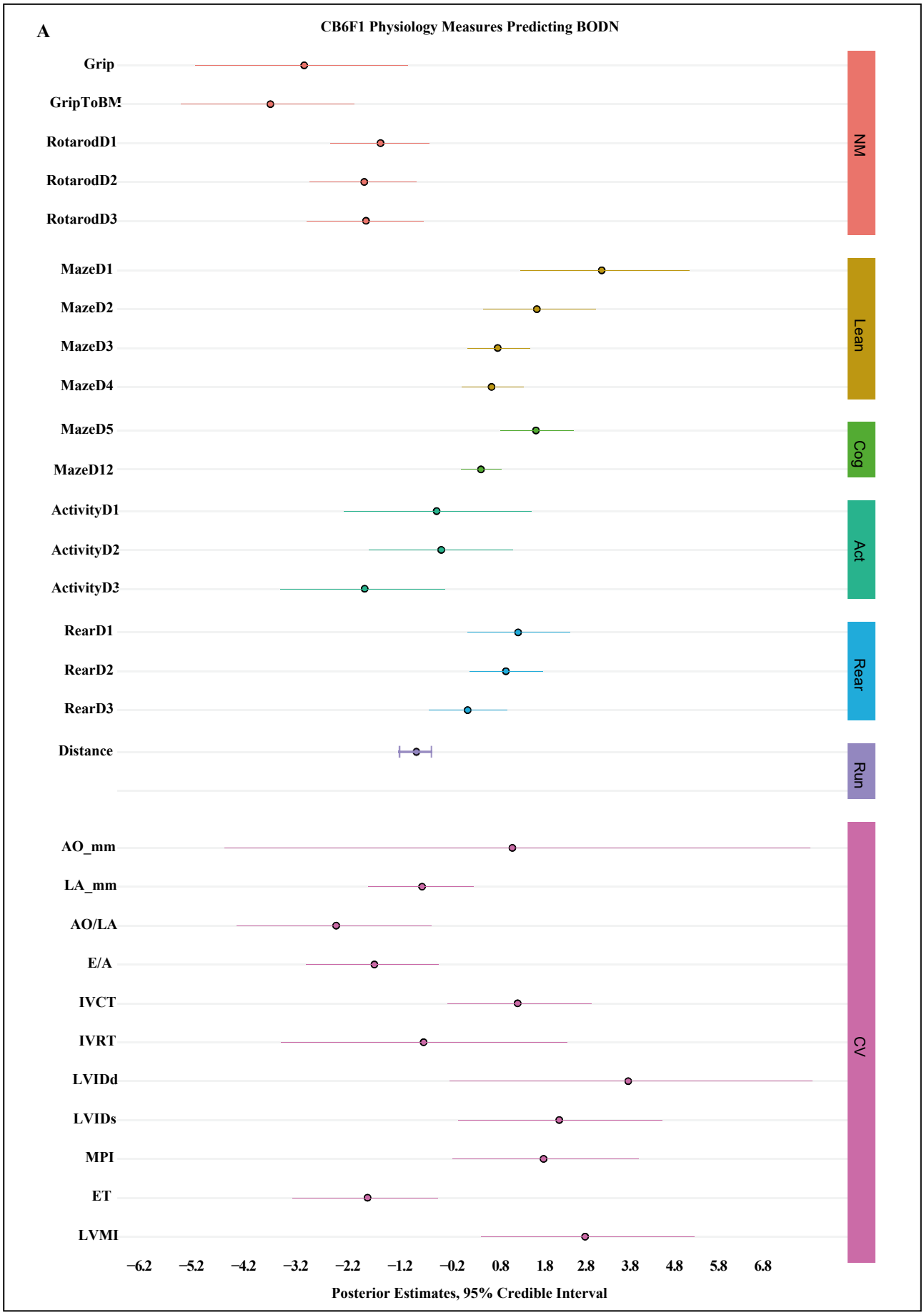

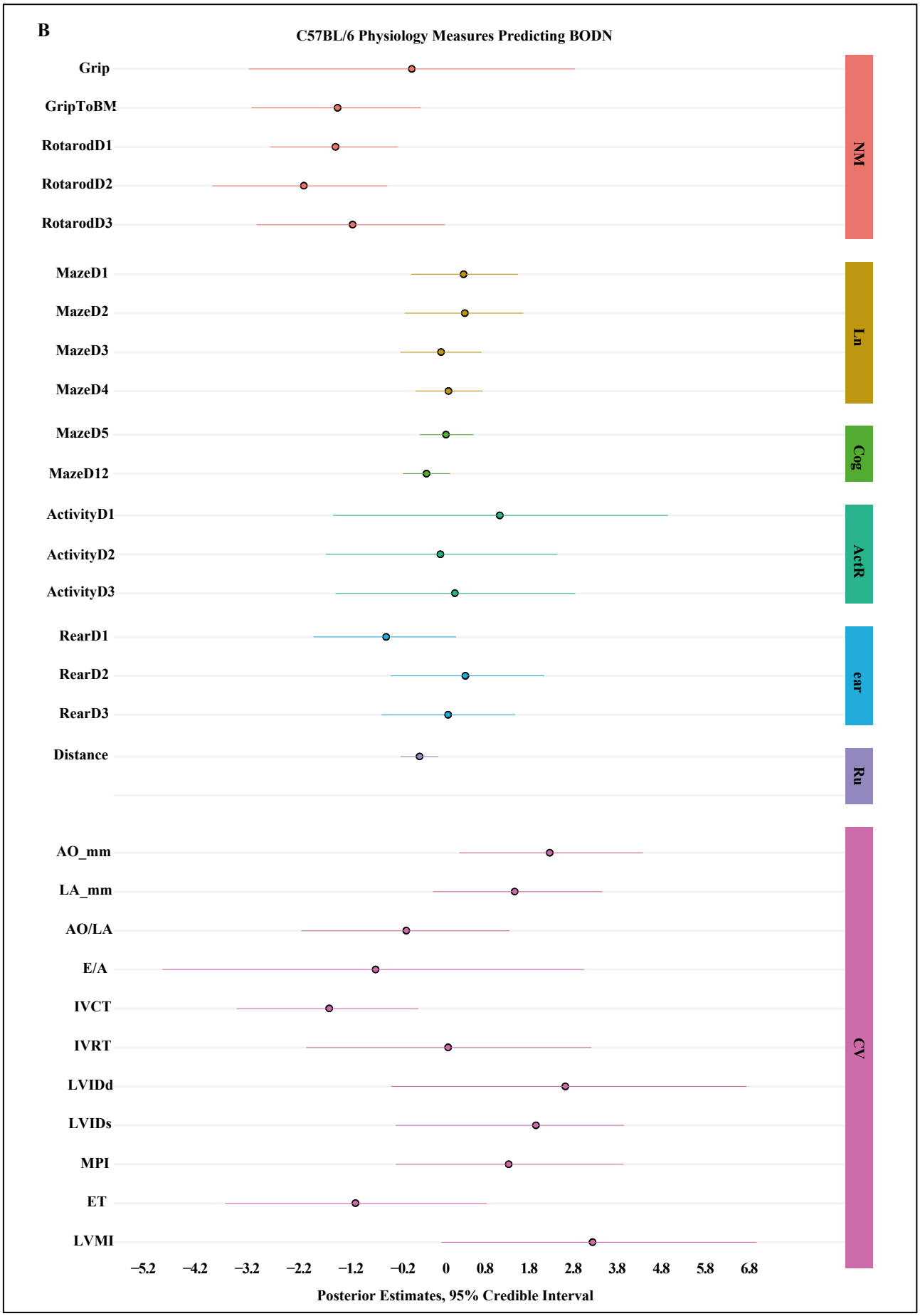
B
C57BL/6 Physiology Measures Predicting BODN
Grip
GripToBM
RotarodD1
RotarodD2
RotarodD3
MazeD1
MazeD2
MazeD3
MazeD4
MazeD5
MazeD12
ActivityD1
ActivityD2
ActivityD3
RearD1
RearD2
RearD3
Distance
AO_mm
LA_mm
AO/LA
E/A
IVCT
IVRT
LVIDd
LVIDs
MPI
ET
LVMI
NM
Ln
Cog
ActR
ear
Ru
CV
−5.2
−4.2
−3.2
−2.2
−1.2
−0.2
0
0.8
1.8
2.8
3.8
4.8
5.8
6.8
Posterior Estimates, 95% Credible Interval

Figure 1. Physiologic predictors of Body Organ Disease Number (BODN) in A) CB6F1, B) C57BL/6 mice. Grip: Grip strength, GriptoBM: normalized grip strength to body size, RotarodD1: rotarod at day 1, MazeD1: Barnes maze at day 1, ActivityD 1: Open field activity at day 1, Rear: Open field activity rearing, AO: aortic valve dimension in millimeter, LA: left ventricular valve, AO/LA: the ratio of AO to LA dimensions, E/A, E wave to A wave ratio, IVCT: isovolumic contractile time millisecond (msec), IVRT: isovolumic relaxation time (msec), LVIDd: left ventricle internal diameter end diastole, IVIDs: left ventricle intra diameter end systole, MPI: myocardial performance, ET: ejection time., NM: neuromuscular, learn: learning stage, Cog: cognition, Act: Open field activity, Rear: Open field activity rearing, Run: Voluntary wheel running, CV: Cardiovascular physiology, LVMI: left ventricular mass index.

Table 1A. Physiologic predictors of Body Organ Disease Number (BODN) in CB6F1 mice.

Physiologic Measures		Coeff	SE	Low 95% CI	Up 95% CI
	Grip	-2.97	1.13	-5.26	-0.81
	Grip to body mass	-3.68	0.93	-5.56	-1.93
Neuromuscular	Rotarod Day 1	-1.38	0.53	-2.43	-0.37
	Rotarod Day 2	-1.72	0.57	-2.86	-0.63
	Rotarod Day 3	-1.69	0.62	-2.93	-0.48
	Maze Day 1	3.24	0.90	1.53	5.07
Learning	Maze Day 2	1.89	0.59	0.76	3.12
	Maze Day 3	1.072	0.33	0.44	1.74
	Maze Da 4	0.94	0.33	0.31	1.61
Cognition	Maze Day 5	1.87	0.39	1.13	2.67
	Maze Day 12	0.72	0.22	0.30	1.16
	Activity Day 1	-0.21	1.002	-2.16	1.77
Physical activity	Activity Day 2	-0.11	0.77	-1.63	1.38
	Activity Day 3	-1.71	0.87	-3.47	-0.03
Rearing Day 1	Rear Day 1	1.49	0.55	0.44	2.59
Rearing Day 2	Rear Day 2	1.24	0.39	0.49	2.02
Rearing Day 3	Rear Day 3	0.44	0.42	-0.38	1.27
Running distance	Distance	-0.63	0.16	-0.98	-0.32
	AO (mm)	1.38	3.13	-4.64	7.62
	LA (mm)	-0.51	0.56	-1.64	0.56
	AO/LA	-2.31	1.03	-4.39	-0.32
	E/A	-1.50	0.70	-2.93	-0.16
	IVCT	1.49	0.76	0.02	3.03
Cardiac Physiology	IVRT	-0.48	1.53	-3.47	2.52
	LVIDd	3.80	1.93	0.07	7.66
	LVIDs	2.36	1.09	0.24	4.52
	MPI	2.03	0.99	0.12	4.01
	ET	-1.65	0.78	-3.23	-0.18
	LVMI	2.90	1.14	0.72	5.19

Grip: Grip strength, Grip to body mass: normalized grip strength to body size, Rotarod Day 1: rotarod at day 1, Maze Day 1: Barnes maze at day 1, Activity Day 1: Open field activity at day 1, Rear: Open field activity rearing, AO: aortic valve dimension in millimeter, LA: left ventricular valve, AO/LA: the ratio of AO to LA dimensions, E/A, E wave to A wave ratio, IVCT: isovolumic contractile time millisecond (msec), IVRT: isovolumic relaxation time (msec), LVIDd: left ventricle internal diameter end diastole, IVIDs: left ventricle intra diameter end systole, MPI: myocardial performance, ET: ejection time., Rearing: Open field activity rearing, Running distance: Voluntary wheel running, LVMI: left ventricular mass index.

Table 1B. Physiologic predictors of Body Organ Disease Number (BODN) in C57BL/6 mice.

Physiologic Measures		Coeff	SE	Low 95% CI	Up 95% CI
	Grip	-0.26	1.54	-3.30	2.78
	Grip to body mass	-1.64	0.80	-3.24	-0.09
Neuromuscular	Rotarod Day 1	-1.68	0.60	-2.90	-0.52
	Rotarod Day 2	-2.27	0.83	-3.98	-0.72
	Rotarod Day 3	-1.36	0.90	-3.15	0.36

Learning	Maze Day 1	0.71	0.50	-0.27	1.72
	Maze Day 2	0.73	0.56	-0.39	1.81
	Maze Day 3	0.29	0.38	-0.47	1.03
	Maze Da 4	0.42	0.32	-0.19	1.06
Cognition	Maze Day 5	0.38	0.26	-0.12	0.89
	Maze Day 12	0.01	0.22	-0.42	0.45
Physical activity	Activity Day 1	1.38	1.59	-1.73	4.51
	Activity Day 2	0.27	1.10	-1.86	2.45
	Activity Day 3	0.55	1.13	-1.68	2.78
Rearing Day 1	Rear Day 1	-0.74	0.68	-2.09	0.56
Rearing Day 2	Rear Day 2	0.74	0.73	-0.66	2.20
Rearing Day 3	Rear Day 3	0.42	0.64	-0.82	1.67
Running distance	Distance	-0.11	0.18	-0.47	0.23
Cardiac Physiology	AO (mm)	2.31	0.87	0.62	4.05
	LA (mm)	1.66	0.80	0.13	3.29
	AO/LA	-0.36	0.99	-2.32	1.56
	E/A	-0.93	1.98	-4.91	2.95
	IVCT	-1.80	0.85	-3.52	-0.14
	IVRT	0.41	1.35	-2.23	3.08
	LVIDd	2.60	1.69	-0.64	5.98
	LVIDs	2.05	0.92	-0.56	3.69
	MPI	1.55	1.09	-0.56	3.69
	ET	-1.31	1.23	-3.74	1.14
	LVMI	3.11	1.49	0.29	6.16

Grip: Grip strength, Grip to body mass: normalized grip strength to body size, Rotarod Day 1: rotarod at day 1, Maze Day 1: Barnes maze at day 1, Activity Day 1: Open field activity at day 1, Rear: Open field activity rearing, AO: aortic valve dimension in millimeter, LA: left ventricular valve, AO/LA: the ratio of AO to LA dimensions, E/A, E wave to A wave ratio, IVCT: isovolumic contractile time millisecond (msec), IVRT: isovolumic relaxation time (msec), LVIDd: left ventricle internal diameter end diastole, IVIDs: left ventricle intra diameter end systole, MPI: myocardial performance, ET: ejection time., Rearing: Open field activity rearing, Running distance: Voluntary wheel running, LVMI: left ventricular mass index.

and this association was stronger at day 2. Also, cognitive decline was associated with an increase in BODN so that the maze test results at day 5 (beta=0.94, 95% CI= 0.35-1.53) and 12 were strongly predictive of BODN (beta=0.92, 95%CI:0.49-1.38). The model stacking over the models including learning stages showed learning stage at day 1 (weight 62.8%) was a stronger predictor of BODN, and the cognition test at day 5 was stronger than day 12 (weight by 98.6%). Stacking over the learning and cognition test stage models showed that day 1 and day 5 weighed more than other days (model weights for day 1: 19.6%, and day 5: 78.9%). We included these two measures of learning and cognition in the PhysioClock model for CB6F1.

For C57BL/6 mice among learning and cognitive stages of the RWT maze test, day 1 and day 5 were the more robust predictors of BODN with model weights 61.5% and 99%, respectively. However, overall, the maze test in C57BL/6 was less predictive of BODN compared to CB6F1, but we included the day 5 maze test as it carried a larger weight to predict BODN.

Open field physical activity, rearing, and wheel running distance. For CB6F1 mice, open field physical activity indicated physical aptitude at day 3 significantly and inversely predicted BODN (beta = -1.7, 95% CI: -3.4 to -0.03). The higher rearing in physical activity, the larger the BODN was with a larger estimate at day 1 (beta = 1.49, 95% CI: 0.44-2.59). However, the model weight favored the rearing activity at day 2 in prediction BODN weighed by 77.2% compared to day 1 (22.8%). We included day 2 rearing activity in the final model determining PhysioClock. The mice with lower running distance had larger system morbidity measured by BODN (beta = -0.6, 95% CI: -0.98 to -0.3).

For C57BL/6 mice, open field physical activity was not significantly predictive of BODN. Stacking the models showed day 1 open field activity model weight was 79.8%. Also, the rearing activity model at day 1 with 57.4% weight explained BODN better than day 2 and 3. The total distance for the running wheel was inversely associated with BODN yet with a broad uncertainty (beta = -0.11, 95% CI = -0.46 to 0.23). We only included total distance in the final model to quantify PhysioClock.

Organ pathology heterogeneously integrates into body organ disease number

Overall, the BODN was higher for CB6F1 than C57BL/6 at any age. The median and range of BODN were 2 (1-4) at 8 months, 4 (2-5) at 16 months, 5 (4-7) at 24 months, 6 (5-7) at 32 months for CB6F1;and for C57BL/6 they were 3 (2-4) at 8 months, 5 (4-6) at 16 months, 5 (4-7) at 24 months, 6 (4-7) at 32 months.

Because the pathologies are ordinally graded based on severity, we used the monotonic effect that is applicable when the levels are not equidistant, and we showed that each organ's pathology severity scores heterogeneously incorporated into body organ disease number (BODN). The result shows that the degree of organ pathology heterogeneously incorporated into BODN in both B6F1and C57BL/6 mice and some pathologies are more dominant for each strain (Figure 2A-B, Table 2A-B).

We included all pathologies that predict BODN with high accuracy using LOO-CV (k < 7). The estimates of each pathology level incorporated into BODN are depicted in Figure 2A and B.

The complete model including all organs' pathology to predict BODN explained variability of BODN by 87% and 88% for C57BL/6 and CB6F1, respectively. We quantified PathoClock from the model, including all organ systems to predict BODN using age as levels. There is intermouse variability of PathoClock even within the same chronological age. Mean PathoClock was mainly larger in CB6F1 compared to C57BL/6, especially at age 28 months (6.5 ± 1.10 *vs*. 6.3 ± 0.64) and 32 months (7.6 ± 1.5 *vs*. 7.3 ± 0.65), respectively. The between-strain variability (variance) over the age spectrum was 3.3 months. In CB6F1, cardiovascular-related pathologies with higher uncertainty (the narrow credible intervals excluding 0) were significantly incorporated into BODN (Figure 2A, Table 2A).

While specific pathologies of each organ variably incorporate into BODN of the renal system, only kidney mineral disposition had a wide uncertainty in CB6F1. In the C57BL/6 mice, in addition to mineral disposition, amyloid accumulation and acute tubular damage had wide credible intervals and large uncertainty predicting BODN (Figure 2B, Table 2B). In C57BL/6, the majority of liver-related pathologies were incorporated into BODN yet heterogeneously. Of note, incorporation of the regeneration state in BODN in C57BL/6 mice was larger than of the degeneration state. Interestingly, lymphoid aggregates in almost all organs are significantly incorporated into BODN.

Correlation of pathoClock, physioClock, and chronological age is strain dependent

To understand how well the two final models, the one including all pathology levels to develop PathoClock and the one including physiology measures to quantify PhysioClock, explained BODN, we used the Leave-One-Out R-squared (LOO_R2) method. The model including all pathologies to predict BODN for C57BL/6 (PathoClock), explained about 87% of BODN (LOO_ R2 = 0.87), while the model used to develop PhysioClock explained BODN by 64% (LOO_R2 = 0.64). For CB6F1 mice the models to develop PathoClock explained BODN by 94% (LOO_R2 = 0.94), and the model used to develop PhysioClock explained BODN by 67% (LOO_R2 = 0.67). In both strains the models from which PathoClock was extracted explained BODN better than PhysioClock; however, in CB6F1 the overall model performance was better than in C57BL/6.

The distributions of PathoClock and PhysioClock are depicted in interactive Figure 3. The correlation of PathoClock and chronological age was $r = 0.75$ in C57BL/6, but in CB6F1 the correlation was larger ($r = 0.80$) (Table 3). In some individual mice, PathoClock was smaller than BODN, while in some mice, it was larger. These results suggest variability in incorporating pathology levels in the same age group and across ages. Also, a larger impact for pathology levels can be manifested as a larger PathoClock in mice within the same age group or in an older group. In contrast, a smaller PathoClock at an older age may suggest the minor impact of pathology levels on BODN despite an older age. This result opens a roadmap to study resilience and body system reactions in relation to pathology (Figure 3A-B).

Correlation between PhysioClock and age at euthanasia in CB6F1 mice was $r = 0.71$ with variability across age groups by 3.72 months (sd = 3.7), and the correlation of PhysioClock with age at euthanasia was $r = 0.68$ for C57BL/6 with 6.5 months variability in age (sd = 6.5; Table 3). Some mice with higher BODN had lower PhysioClock (at middle age), suggesting physiological resilience to the development of pathology. However, it could also be due to an insufficient adaptation response. Despite the high correlation, the patterns of both PathoClock and PhysioClock in relation to chronological age were not linear, and exponential patterns were detected (Figure 3C-D).

PhyisoAge and PathoAge align with chronological age in a strain dependent manner

The common approach to measuring the rate of aging with chronological age has been to regress phenotype measurements over chronological age. Likewise, we developed PhysioAge and PathoAge by regressing the physiological and pathological measurements on chronological age and determining the R2 of the model using the Leave-One-Out approach (LOO_R2) and then assessing the correlation between predicted age and chronological age for PathoAge and PhysioAge. In C57BL/6 mice, PathoAge, having a larger LOO_R2 and stronger correlation with chronological age, explained chronological age better than PhsyioAge. PathoAge variability across age was 2.5 months while the variability of PhysioAge was 3.9 months (Table 3). In CB6F1, both PathoAge and PhysioAge strongly explained chronological age, with PathoAge (LOO_R2 = 0.93) explaining chronological age better than PhysioAge (Loo_R2 = 0.7). In C57BL/6 mice, there was a slow slope of correlation between PhysioAge and ChAge so that the PhysioAge at younger ages had similarities with middle age groups (Figure 4).

RESEARCH

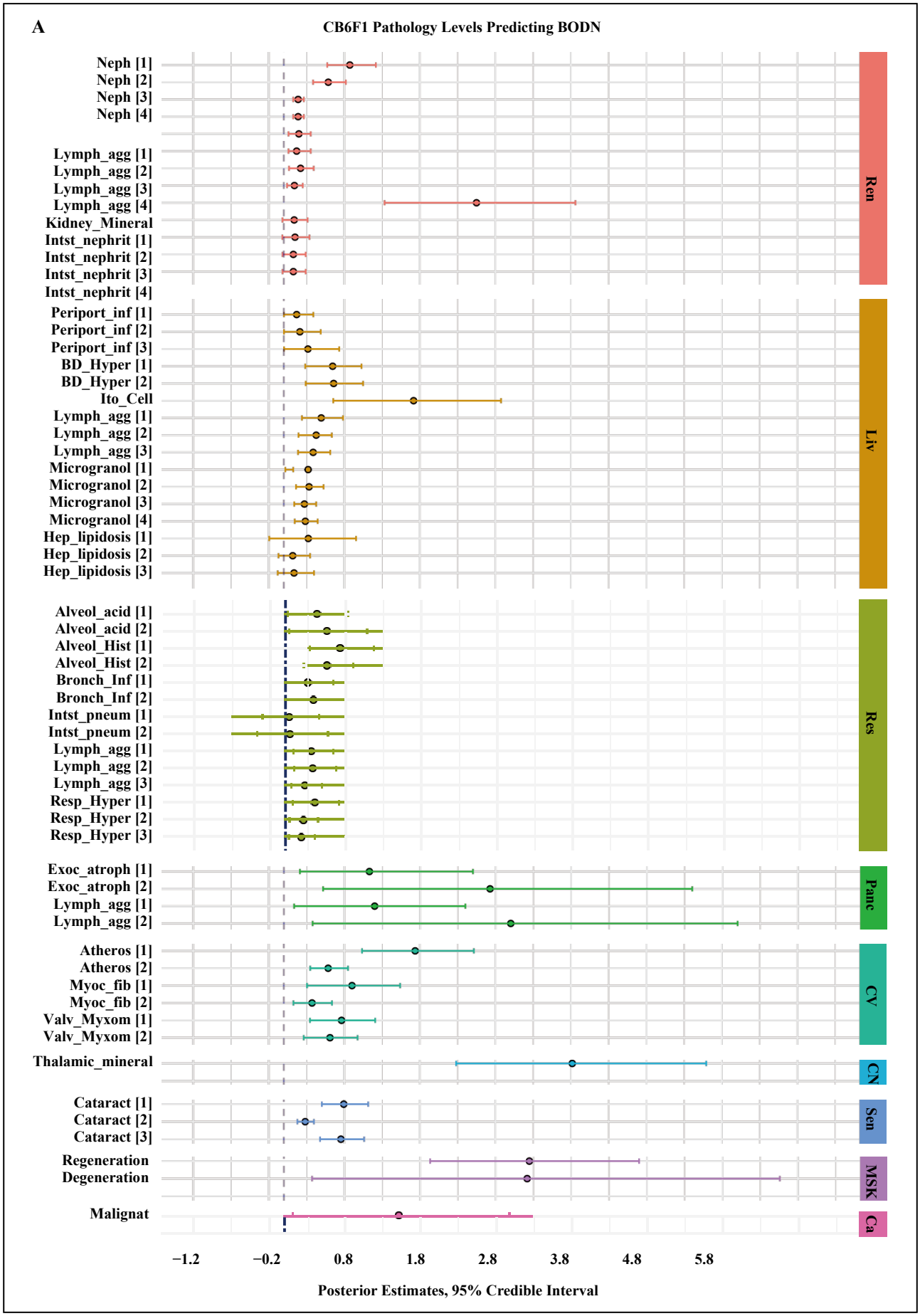
A
CB6F1 Pathology Levels Predicting BODN
Neph [1]
Neph [2]
Neph [3]
Neph [4]
Lymph_agg [1]
Lymph_agg [2]
Lymph_agg [3]
Lymph_agg [4]
Kidney_Mineral
Intst_nephrit [1]
Intst_nephrit [2]
Intst_nephrit [3]
Intst_nephrit [4]
Ren
Periport_inf [1]
Periport_inf [2]
Periport_inf [3]
BD_Hyper [1]
BD_Hyper [2]
Ito_Cell
Lymph_agg [1]
Lymph_agg [2]
Lymph_agg [3]
Microgranol [1]
Microgranol [2]
Microgranol [3]
Microgranol [4]
Hep_lipidosis [1]
Hep_lipidosis [2]
Hep_lipidosis [3]
Liv
Alveol_acid [1]
Alveol_acid [2]
Alveol_Hist [1]
Alveol_Hist [2]
Bronch_Inf [1]
Bronch_Inf [2]
Intst_pneum [1]
Intst_pneum [2]
Lymph_agg [1]
Lymph_agg [2]
Lymph_agg [3]
Resp_Hyper [1]
Resp_Hyper [2]
Resp_Hyper [3]
Res
Exoc_atroph [1]
Exoc_atroph [2]
Lymph_agg [1]
Lymph_agg [2]
Panc
Atheros [1]
Atheros [2]
Myoc_fib [1]
Myoc_fib [2]
Valv_Myxom [1]
Valv_Myxom [2]
CV
Thalamic_mineral
CN
Cataract [1]
Cataract [2]
Cataract [3]
Sen
Regeneration
Degeneration
MSK
Malignat
Ca
−1.2
−0.2
0.8
1.8
2.8
3.8
4.8
5.8
Posterior Estimates, 95% Credible Interval

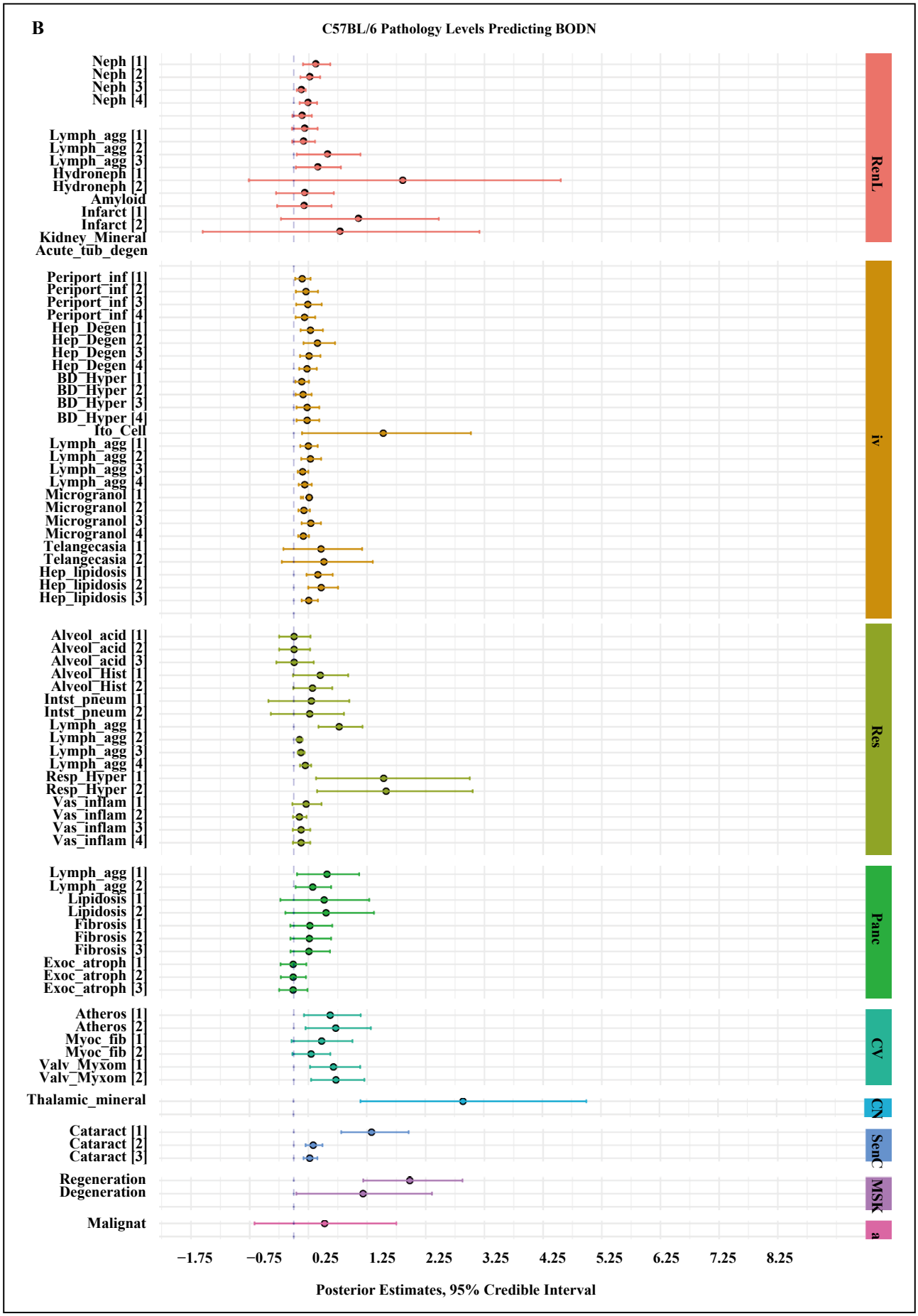

Figure 2. Pathology levels of seven organs in A) CB6F1 and B) C57BL/6 male mice incorporating Body Organ Disease Number. Abbreviations: Neph: nephropathy, lymph_agg: lymphocyte aggregation, Infarct: infarction, Kidney_mineral: mineral deposition in kidney, Acute, tub_degen: acute tubular degeneration, perioport_inf: periportal infiltration, Hep_Degen: hepatic degeneration, BD_Hyper: bile duct hyperplasia, Ito_cell: itocell hyperplasia, Microgranol: microgranuloma, Hep_lipidosis: hepatic lipidosis, Alveol acid: alveolar macrophage pneumonia, alveol_hist: alveolar histiocytosis, Resp_hyper: respiratory duct hyperplasia, Vas_inflam: perivascular inflammation, exoc_atroph: exocrine atrophy, Atheros: atherosclerosis, Myco_fib: myocardial fibrosis, Valve_Myxom: valvular myxomatosis, thalamic mineral: mineral deposition in thalamus area, Regeneration: skeletal muscle degeneration, regeneration: skeletal muscle regeneration, malignant: malignant cancer. All the pathology levels are compared to no lesions [0] as the reference.

Table 2A. Organ system histology levels predicting Body Organ Disease Number in CB6F1 mice.

Systems	Disease	Beta Coeff	SE	Low 95% CI	Up 95% CI
Renal	Nephropathy [1]	0.8740	0.1610	0.5750	1.2190
	Nephropathy [2]	0.5890	0.5890	0.3875	0.8215
	Nephropathy [3]	0.1900	0.0340	0.1260	0.2650
	Nephropathy [4]	0.1910	0.036	0.1280	0.2670
	Lymph aggregate [1]	0.1998	0.0729	0.0621	0.3564
	Lymph aggregate [2]	0.1702	0.0621	0.0621	0.3564
	Lymph aggregate [3]	0.2220	0.0810	0.0690	0.3960
	Lymph aggregate [4]	0.1406	0.0513	0.0437	0.2508
	Kidney Mineralization [1]	2.5510	0.6481	1.3340	3.8607
	Interstitial nephritis [1]	0.1375	0.0825	-0.0175	0.3150
	Interstitial nephritis [2]	0.1485	0.0891	-0.0189	0.3402
	Interstitial nephritis [3]	0.1265	0.0759	-0.0161	0.2898
	Interstitial nephritis [4]	0.1265	0.0429	-0.0161	0.2898
Liver	Periportal inflammation [1]	0.1704	0.0984	0.00216	0.3912
	Periportal inflammation [2]	0.2130	0.1230	0.0027	0.4890
	Periportal inflammation [3]	0.3195	0.1845	0.0036	0.7330
	Bile duct hyperplasia [1]	0.6468	0.1862	0.2842	1.0290
	Bile duct hyperplasia [2]	0.6600	0.1900	0.2900	1.0500
	Ito Cell hyperplasia [1]	1.7182	0.5664	0.6549	2.8760
	Lymph aggregate [1]	0.4958	0.1369	0.2405	0.7844
	Lymph aggregate [2]	0.4288	0.1184	0.1950	0.6360
	Lymph aggregate [3]	0.3886	0.1073	0.1885	0.6148
	Microgranular aggregate [1]	0.3224	0.0858	0.0208	0.1248
	Microgranular aggregate [2]	0.3348	0.0891	0.1620	0.5265
	Microgranular aggregate [3]	0.2728	0.0726	0.1386	0.4290
	Microgranular aggregate [4]	0.2852	0.0759	0.1449	0.4485
	lipidosis [1]	0.3245	0.3025	-0.1925	0.9570
	lipidosis [2]	0.1180	0.1100	-0.0700	0.3480
	lipidosis [3]	0.1357	0.1265	-0.0805	0.4002
Respiratory	Alveolar acidosis [1]	0.4343	0.2021	0.0473	0.8428
	Alveolar acidosis [2]	0.5656	0.2632	0.0616	1.0976
	Alveolar histiocytosis [1]	0.7392	0.2128	0.3360	1.1872
	Alveolar histiocytosis [2]	0.5676	0.1634	0.2580	0.9116
	Bronchial Inflammation [1]	0.3124	0.1672	0.00004	0.6512
	Bronchial Inflammation [2]	0.3850	0.2090	0.00006	0.814
	Inessential pneumonia [1]	0.0616	0.1892	-0.2904	0.462
	Interstitial pneumonia [2]	0.0770	0.2365	-0.3630	0.5775
	Lymph aggregate [1]	0.3535	0.1295	0.1225	0.6475
	Lymph aggregate [2]	0.3737	0.1369	0.1295	0.6845
	Lymph aggregate [3]	0.2727	0.0999	0.0945	0.4995
	Respiratory hyperplasia [1]	0.4005	0.1530	0.1080	0.7245
	Respiratory hyperplasia [2]	0.2492	0.0952	0.0672	0.4480
	Respiratory hyperplasia [3]	0.2225	0.0850	0.0600	0.4000
Pancreas	Exocrine atrophy [1]	1.0640	0.8596	0.2044	3.5000
	Exocrine atrophy [2]	1.3490	1.08985	0.25915	4.4375
	Lymph aggregate [1]	0.9360	0.7930	0.1352	3.1200
	Lymph aggregate [2]	1.3140	1.1132	0.1898	4.3800

CV	Atherosclerosis [1]	1.7390	0.3700	1.0300	2.5100
	Atherosclerosis [2]	0.5875	0.1250	0.3500	0.8500
	Fibrosis [1]	0.9030	0.3080	0.3080	1.5400
	Fibrosis [2]	0.3741	0.1276	0.1276	0.638
	Valve myxoma [1]	0.7645	0.2200	0.3465	1.2100
	Valve myxoma [2]	0.6116	0.1760	0.2640	0.9768
CNS	Thalamic mineralization [1]	3.8187	0.8417	2.2818	5.5921
Sensory	Cataract [1]	0.7938	0.1512	0.504	1.1172
	Cataract [2]	0.2835	0.0540	0.1800	0.3990
	Cataract [3]	0.7560	0.1440	0.4800	1.0640
Muscle	Muscle regeneration [1]	3.2460	0.7061	1.9342	4.6973
	Muscle degeneration [1]	3.2169	1.5585	0.3723	6.5585
Pancreas	Exocrine atrophy [1]	1.0640	0.8596	0.2044	3.5000
	Exocrine atrophy [2]	1.3490	1.08985	0.25915	4.4375
	Lymph aggregate [1]	0.9360	0.7930	0.1352	3.1200
	Lymph aggregate [2]	1.3140	1.1132	0.1898	4.3800
Cancer	Any malignant tumor [1]	1.5186	0.7279	0.1156	2.9808

SE: Standard error, CV: cardiovascular system, CNS: central nervous system.

Table 2B. Organ system histology levels predicting Body Organ Disease Number in C57BL/6 mice.

Systems	Diseases	Coeff	SE	Low 95% CI	Up 95% CI
Renal	Nephropathy [1]	0.3672	0.1152	0.1584	0.6228
	Nephropathy [2]	0.2652	0.0780	0.1144	0.4498
	Nephropathy [3]	0.1224	0.0384	0.0528	0.2041
	Nephropathy [4]	0.2346	0.0736	0.1012	0.3979
	Lymph aggregation [1]	0.1344	0.0840	-0.0224	0.3080
	Lymph aggregation [2]	0.1776	0.1110	-0.0296	0.4070
	Lymph aggregation [3]	0.1584	0.0990	-0.0264	0.3630
	Hydronephrosis [1]	0.5684	0.2726	0.0522	1.1368
	Hydronephrosis [2]	0.4018	0.1927	0.0369	0.8036
	Amyloidosis	1.8581	1.3438	-0.7660	4.5509
	Infarction [1]	0.1785	0.2499	-0.3009	0.6834
	Infarction [2]	0.1680	0.2352	-0.2832	0.6432
	Kidney mineralization	1.0949	0.6853	-0.2180	2.4723
	Tubular degeneration	0.7806	1.2956	-1.7512	3.3652
Liver	Periportal infiltration [1]	0.1440	0.0648	0.0252	0.2862
	Periportal infiltration [2]	0.2080	0.2080	0.0364	0.4134
	Periportal infiltration [3]	0.2400	0.1080	0.0420	0.4770
	Periportal infiltration [4]	0.1840	0.0828	0.0322	0.3657
	Hepatic degeneration [1]	0.2856	0.0960	0.1176	0.4968
	Hepatic degeneration [2]	0.4046	0.1360	0.1666	0.7038
	Hepatic degeneration [3]	0.2618	0.0880	0.1078	0.4554
	Hepatic degeneration [4]	0.2261	0.0760	0.0931	0.3933
	Bile Duct hyperplasia [1]	0.1368	0.0576	0.0288	0.2610
	Bile Duct hyperplasia [2]	0.1596	0.0672	0.0336	0.3045
	Bile Duct hyperplasia [3]	0.2280	0.0960	0.0480	0.4350
	Bile Duct hyperplasia [4]	0.2280	0.0960	0.0480	0.4350
	Ito Cell hyperplasia	1.5260	0.7330	0.1411	3.0196
	Lymph aggregation [1]	0.2492	0.0756	0.1120	0.4088
	Lymph aggregation [2]	0.2848	0.0864	0.1208	0.4672
	Lymph aggregation [3]	0.1513	0.0459	0.0680	0.2482

	Lymph aggregation [4]	0.1869	0.0567	0.0840	0.3066
	microgranuloma [1]	0.2639	0.0754	0.1218	0.1595
	microgranuloma [2]	0.1729	0.0494	0.0798	0.2755
	microgranuloma [3]	0.2912	0.0832	0.1344	0.4640
	microgranuloma [4]	0.1638	0.0468	0.0756	0.2610
	Telangiectasia [1]	0.4653	0.3525	-0.1755	1.1655
	Telangiectasia [2]	0.5148	0.3901	-0.2028	1.3468
	Hepatic lipidosis [1]	0.4118	0.1131	0.2175	0.6641
	Hepatic lipidosis [2]	0.4686	0.1287	0.2475	0.7557
	Hepatic lipidosis [3]	0.2556	0.0702	0.135	0.4122
	Hepatic lipidosis [1]	0.4118	0.1131	0.2175	0.6641
	Hepatic lipidosis [2]	0.4686	0.1287	0.2475	0.7557
	Hepatic lipidosis [3]	0.2556	0.0702	0.135	0.4122
	Alveolar histiocytosis [1]	0.4524	0.2378	-0.0116	0.9280
	Alveolar histiocytosis [2]	0.3198	0.1681	-0.0082	0.6560
	Interstitial pneumonia [1]	0.3016	0.3276	-0.4316	0.9464
	Interstitial pneumonia [2]	0.2726	0.2961	-0.3901	0.8554
	Lymph aggregation [1]	0.7749	0.1890	0.4221	1.1718
Respiratory	Lymph aggregation [2]	0.0984	0.0240	0.0536	0.1488
	Lymph aggregation [3]	0.1230	0.0301	0.0670	0.1860
	Lymph aggregation [4]	0.1968	0.0480	0.1072	0.2976
	Respiratory Hyperplasia [1]	1.5328	1.0560	0.3808	3.9001
	Respiratory Hyperplasia [2]	1.5745	1.1055	0.3986	4.3550
	Vascular inflammation [1]	0.2109	0.1221	-0.0222	0.4736
	Vascular inflammation [2]	0.0969	0.0561	-0.0119	0.2176
	Vascular inflammation [3]	0.1254	0.0726	-0.0154	0.2816
	Vascular inflammation [4]	0.1254	0.0726	-0.0132	0.2816
	Lymph aggregation [1]	0.5670	0.2646	0.0567	1.1151
	Lymph aggregation [2]	0.3240	0.1512	0.0324	0.6372
	Lipidosis [1]	0.5184	0.3601	-0.2272	1.2864
	Lipidosis [2]	0.5508	0.3825	-0.1428	1.3668
Pancreas	Fibrosis [1]	0.2754	0.1802	-0.0578	0.6562
	Fibrosis [2]	0.2673	0.1749	-0.0561	0.6369
	Fibrosis [3]	0.2592	0.1696	-0.0544	0.6176
	Exocrine atrophy [1]	-0.0096	0.1120	-0.2240	0.2144
	Exocrine atrophy [2]	-0.0093	0.0527	-0.2201	0.2077
	Exocrine atrophy [3]	-0.0105	0.1225	-0.2485	0.2345
	Atherosclerosis [1]	0.6210	0.2438	0.1748	1.1408
	Atherosclerosis [2]	0.7155	0.2809	0.2014	1.3144
CV	Myocardial fibrosis [1]	0.4758	0.2562	-0.0366	1.0004
	Myocardial fibrosis [2]	0.2964	0.1596	-0.0228	0.6232
	Valvular myxomatosis [1]	0.6768	0.2160	0.2784	1.1328
	Valvular myxomatosis [2]	0.7191	0.2295	0.2958	1.2036
CNS	Thalamic mineralization	2.8945	1.2855	1.1442	5.9831
	Cataract [1]	1.3260	0.2924	0.8092	1.9584
Sensory	Cataract [2]	0.3315	0.0731	0.2023	0.4896
	Cataract [3]	0.2730	0.0602	0.1666	0.4032
Muscle	Muscle regeneration [1]	1.9779	0.4315	1.1847	2.8763
	Muscle degeneration [1]	1.1812	0.5901	0.0448	2.3558
Cancer	Any malignant tumor [1]	0.5266	0.6146	-0.6678	1.7486

SE: Standard error, CV: cardiovascular system, CNS: central nervous system.

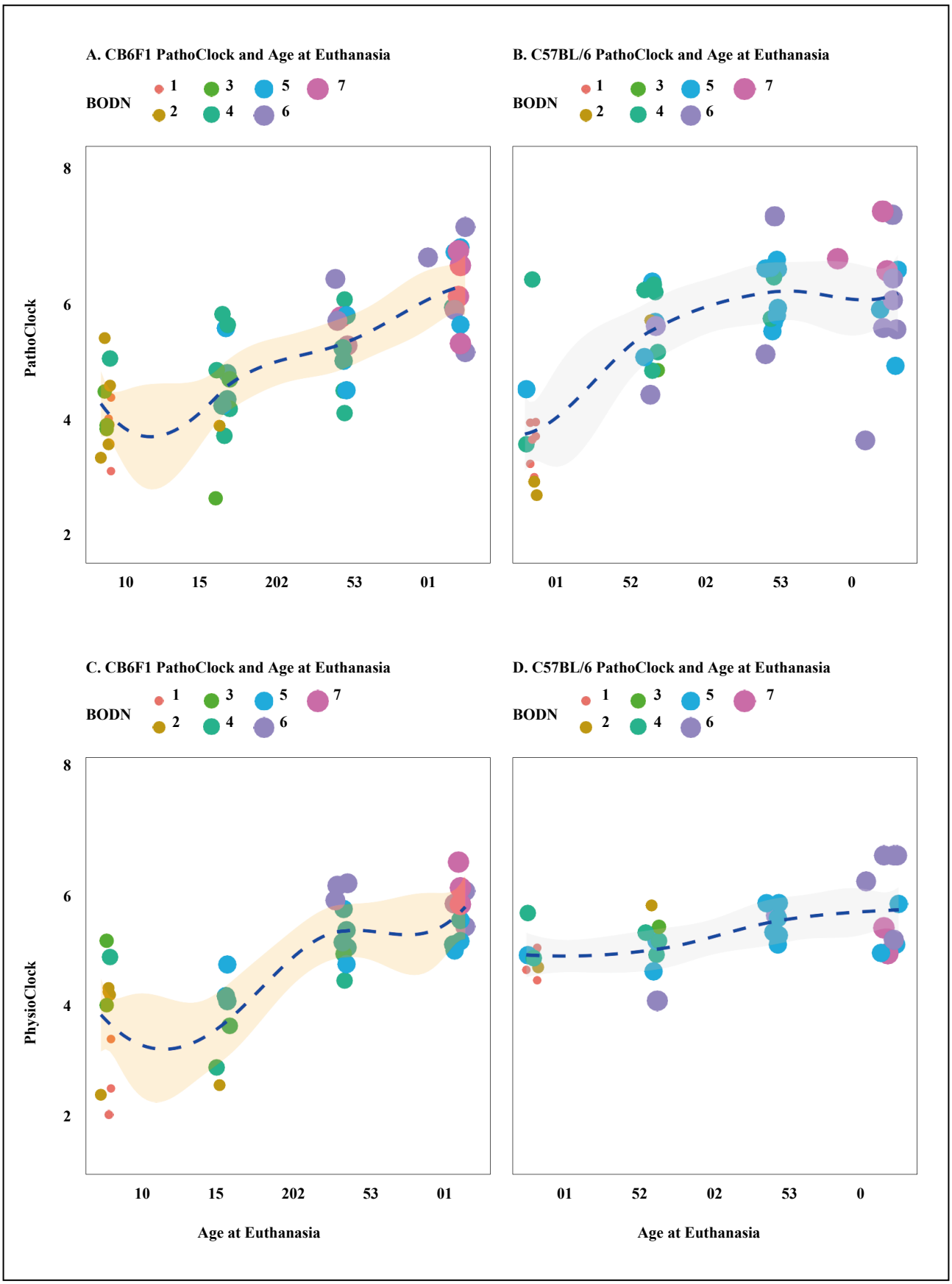

Figure 3. The distribution of PathoClock and PhysioClock by age. To see the 3D figures, click on the included links. PathoClock is determined by how each pathology level incorporates into Body Organ Disease Number (BODN). **A.** PathoClock in CB6F1 mice and age at euthanasia. **B.** PathoClock in C57BL/6 mice and age at euthanasia. PhysioClock was determined by how each physiological measures predicted BODN. **C.** CB6F1 PhysioClock and age at euthanasia. **D.** C57BL/6 PhysioClock and age at euthanasia.

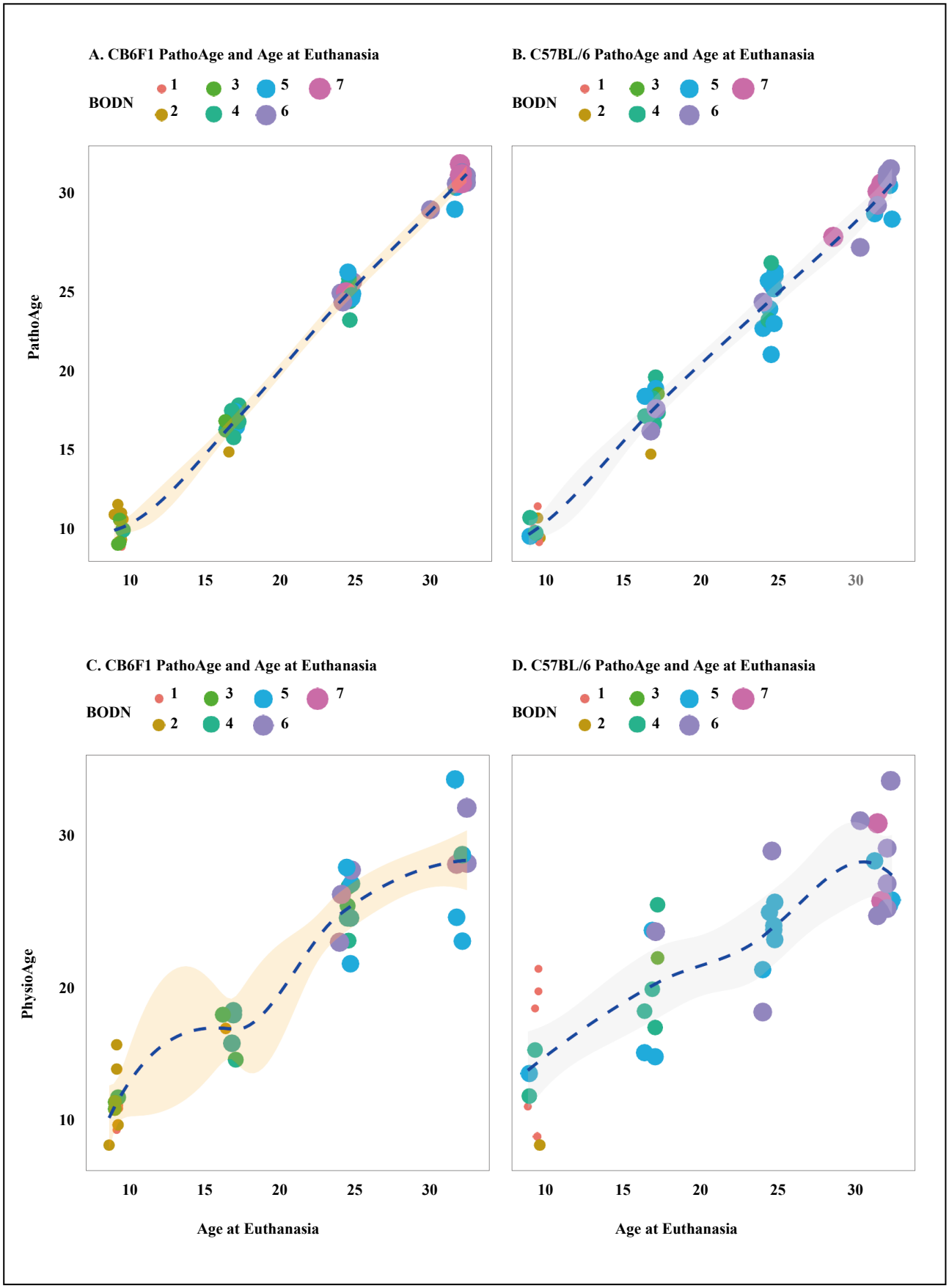

Figure 4. Developing PathoAge, pathologies were included in a model to predict chronological age in both **A**. CB6F1 and **B**. C57BL/6. Developing PhysioAge, the same physiological measures as the ones used in Physioclock, were regressed over chronological age in both **C**. CB6F1 and **D**. C57BL/6. While PathoAge are almost linearly predict chronological age with some subtle degree of uncertainty, PhysioAge in both strains endures more uncertainty to predict chronological age. The size and color indicate the increase in number of body organ disease number (BODN).

Table 3. Leave-One-Out (LOO) R squared of models for developing PathoClock, PhysioClock, PathoAge and PhysioAge and the correlation with chronological age.

	LOO-R2 (Sd or sigma) C57BL/6	Correlation (r) with ChAge (C57BL/6)	LOO-R2 (Sd or sigma) CB6F1	Correlation (r) with ChAge (CB6F1)
Model For PhysioClock	0.87, (sd = 5.7 months)	0.76	0.94, (sd = 7.4 months)	0.80
Model For PhysioClock	0.64, (sd = 6.7 months)	0.68	0.67, (sd = 3.7 months)	0.73
Model for PathoAge	0.86, (sigma = 2.5 months)	0.98	0.93, (sigma = 2 .4 months)	0.98
Model for PhysioAge	0.75, (Sigma = 3.9 months)	0.83	0.70, (Sigma = 4.0 months)	0.93

Sd: standard deviation for model levels in multilevel analyses, sigma is the variance of Gaussian family for continuous outcome. ChAge: Chronological Age.

Discussion

In this study, physiology performance and pathology data were generated from C57BL/6 and CB6F1 male mice ranging from 4 to 28 months of age. As a result of these data, pathology-based multimorbidity as an outcome was developed and is reported for the first time, with the pathological and physiological determinants designated as PathoClock, and PhysioClock, respectively. Using histopathology lesion scores in each organ as a proxy for diseases, the morbidity of each organ system was defined as at least two low pathology grades (= 1) or one higher pathology grade (> 1). The sum of the organ systems' morbidities determined the Body Organ Disease Number (BODN) as a new outcome representing a global index of health at the body organ system level, resembling what was recently developed and validated in a multimorbidity study of human aging [16]. The degree to which each organ-specific pathology level incorporates into BODN was assessed. The mouse strain-specific pathology levels predicting BODN was termed PathoClock, a counterpart of Body Clock in humans [16]. Because physiological responses can vary by age and disease level, BODN was used as an outcome for determining physiological predictors developing PhysioClock which association with chronological age was assessed. The results showed that various levels of the pathology of various organs heterogeneously incorporate into BODN. CB6F1 mice had a larger BODN and PathoClock compared to C57BL/6 mice in the same age group.

Interestingly, the two strains had distinct pathological and physiological components that predicted BODN. While aortic valve (AO) and left atrium (LA) dimensions significantly predicted BODN in C57BL/6 mice, in CB6F1 mice only the AO to LA ratio was a significant predictor of BODN. There was an inverse association of the E/A ratio with BODN in CB6F1. A decreased E/A ratio which is usually an indicator of diastolic heart failure suggests fibrosis so that the left ventricle cannot be filled with blood during the diastolic period between two contractions.

Similarly, heart failure in humans is one of the age-related changes incorporated into BODN [16] and a health burden underlying hospitalization of older adults [35]. Moreover, in older adults decrease in the E/A ratio incorporates into low exercise intolerance. The results in CB6F1 mice showed both an inverse association of voluntary exercise (running distance) and E/A ratio with BODN.

In both strains, while the Left ventricle dimension in end-systole (LVIDs) significantly predicted BODN, the left ventricle dimension in end-diastole (LVIDd) predicted BODN but with larger uncertainty. Shortening ejection time (ET), which has been suggested as a single indicator of human heart failure [36-38] , significantly predicted BODN in CB6F1. A human study of echocardiographic measures has shown that a combination of both systolic and diastolic impairments is a better predictor of heart failure [37], as such a measure like the myocardial performance index (MPI) was a significant predictor of BODN in CB6F1, and it also predicted BODN in C57BL/6, albeit with some uncertainty. Left ventricular hypertrophy index normalized by tibial length (LVMI), an age-related change significantly predicted BODN in both strains. Cardiac physiology markers were associated with BODN more strongly in CB6F1 mice than C57BL/6. Having more uncertainties in cardiac physiology measures, C57BL/6 mice might manifest cardiac physiology changes late in life or have physiological adaptation to histopathological changes later. Although PhysioClocks for both strains were associated with chronological age at euthanasia, the correlation was stronger in CB6F1, and there was larger variability in PhysioClock in C57BL/6 than in CB6F1. Replicative studies and response to interventions are required to replicate cardiac physiology changes in response to pathology.

There was variability in both organ physiology and pathology across strains and age groups. The ability to maintain neuromuscular and cognitive performance is an important component of healthspan in aging. Impaired physical activity and function are both causes and consequences of disease in humans [39]. Albeit heterogeneous, older C57BL/6 mice had uncertainties in physical activity capacity in relation to BODN, while CB6F1 showed decreased balance, physical activity, lower running distance, and lower grip strength, all of which predicted increased BODN. All of these measures had a larger uncertainty in C57BL/6 to predict BODN. One possible explanation for the wider uncertainty of physiologic measures in the prediction of BODN in C57BL/6 is that some male C57Bl/6

mice at age 4 months might have already commenced physiological changes in response to pathology so that they are already similar to middle-aged mice. However, the C57BL/6 PhysioClock at older ages showed a relatively slow slope over the age spectrum which suggests resilience in physical function due to regenerative capacity in skeletal muscle in this strain as shown in their histopathology and association with BODN.

CB6F1 mice showed a more significant cognitive decline, attenuated volitional physical activity, disturbed balance, and diminished motor function in predicting BODN, while such functional measures did not significantly predict BODN in C57BL/6. The results suggest that C57BL/6 are also more resilient to functional decline than CB6F1 and/or might develop functional decline variability. While these two strains are commonly used in the study of normal aging, our results suggest strain-specific variability in pathological and physiological domains. However, mechanisms of functional resilience and whether there is more variability in functional impairment in C57BL/6, despite developing pathologies, can be explored by comparing PathoClock and PhysioClock in both strains and measuring in-depth mechanistic markers in response to anti-aging interventions.

Recent reports in both CB6F1 and C57BL/6 mice show different organ aging, suggesting higher pathology scores in the cardiovascular system in CB6F1 and early onset of liver and kidney aging in C57BL/6 and organ-specific response to anti-aging interventions [40]. Because the aging kidney and liver show early and dominant age-related characteristics in C57BL/6, the inclusion of physiological markers of such organs to predict BODN may improve PhysioClock for both strains. Moreover, adding more organs to pathological studies, and obtaining more information by applying artificial intelligence to the images to extract high throughput information on echocardiography, pathology and other imaging can be incorporated into BODN and can update PathoClock and PhysioClock whenever this information is available.

In both strains, PathoClock was more strongly correlated with chronological age, with the CB6F1 PathoClock having a larger correlation, and we found variability in components of pathology and physiology across age groups. Recently, a new study applied the frailty component on chronological age FRAIL (Frailty Inferred Geriatric Health Timeline) and measuring lifespan with AFRAID (Analysis of Frailty and Death,) in C57BL/6 mice predicted age with $r^2 = 0.64$ in the test data [12]. Our models based on pathology or physiology more significantly predicted the animal's chronological age with PathoAge in both strains and PhysioAge mainly in CB6F1. In addition, PathoClock based on BODN showed a stronger correlation with chronological age (in CB6F1, $r = 0.8$; in C57BL/6, $r = 0.76$), and likewise, PhysioClock had larger correlation with chronological age (CB6F1: $r = 0.73$; C57Bl/6: $r = 0.68$). In both strains, the models from which PathoClock was extracted explained BODN better than PhysioClock, with model performances better for CB6F1 than C57BL/6. Similarly, PathoAge better predicted chronological age than PhysioAge with a larger correlation between observed and predicted chronological age. One possible explanation for the different correlations is the wider variability and uncertainty in physiological measures in predicting BODN and chronological age. Also, the data showed an exponential association between physiological-based predicted age and chronological rather than linear. Another possibility is that we had smaller sample sizes for physiological measurements (30 mice in C57BL/6 and 35 in CB6F1).

In CB6F1 mice, the lower running distance was associated with larger BODN and Maze tests, and physical activity at day 3 and rearing activity at days 1 and 2 were significantly predicted BODN. However, these results were not significant in CB57BL/6. One possible explanation is that functional decline occurs later in life and histopathologic changes in other organs appear sooner, as epidemiological studies have reported in humans. Cognitive decline and disability are mainly saturated late in life. In this study, the mice were euthanized at a specific time, and perhaps longer follow-up can test this surmise. Moreover, there is strain discrepancy so that C57Bl/6 showed more regeneration than degeneration in skeletal muscle, suggesting the regenerative capacity of skeletal muscle maintains the physical activity in this mouse strain. Further studies with longer follow-up time and serial measurements of physical activities in both sexes are required to shed additional light on possible mechanisms underlying these results. To better delineate pattern recognition, replication of these analyses including a larger sample size would be helpful.

The two clocks developed, PathoClock and PhysioClock, are strong healthspan tools. In human aging, metrics that are statistically trained on phenotypes also predict health states [16]. One caveat of basing the data on chronological age is that there is arbitrarily consideration of chronological age as a variable outcome, while chronological age is a fixed number in an equation. Moreover, biomarker-based measures can fluctuate irregularly across age spectrums due to a variety of reasons such as adaptation, resilience, or severe organ damage. However, prediction of health outcomes like BODN can capture biological and pathophysiological changes independent of chronological age, as well as the variability of biological age. While BODN and PathoClock can be used at the endpoint for healthspan, the PhysioClock can be used as a repeated measure in longitudinal studies to predict healthspan over time. The results of previously measured pathologies can be applied in the Bayesian models we developed, along with physiological measures, to predict BODN in aging studies using mice and can be used dynamically to further delineate mechanisms of aging [41]. Including components of pathology and or physiology into the models provides the ability to predict chronological age and integration into global health status measured as BODN. Our study revealed between- and within-age variabilities in PathoClock and PhysioClock, as well as between-strain variabilities.

For the first time, we applied BODN to histopathology and developed PathoClock and PhysioClock to recapitulate human BODN and Body Clock, which can be used to compare the rate of aging across various rodent strains and other mammalian species. Our findings are novel as, for the first time, we employed human BODN histopathology, developing the PathoClock and PathoAge that show the rate of aging independent of chronological age, resembling human BODN and Body Clock. Furthermore, these tools can be used in other mouse strains to compare the rate of aging across various rodent strains and other mammalian species. Considering organ-specific aging in mouse strains and heterogeneity in organ aging in humans, it is of paramount importance to disentangle individual-specific and organ-specific aging and how each disease state and adaptation state incorporates into the whole-body system as a function of BODN. The PathoClock and PhysioClock can be employed as translatable tools, recapitulating the human Body Clock. These clocks can be used across various species and in both males and females to determine common and distinguished pathologies and physiological assessments applied to age-related healthspan.

Impractical pan-organ histopathology studies in humans might limit the translatability of non-human histopathologic tools. One possibility is to compare human organoids with histopathology studies of other species, as the mammalian body systems are one entropy with interactions between systems. Therefore, the study of organoids could limit us from capturing the effect of one organ on others as we captured by BODN. Clinically defined diseases in humans usually track well with underlying histopathologic changes. Thus, determining animal models that can recapitulate clinically defined human multimorbidity is still crucial for translational purposes.

In this study, we applied the human BODN and Body Clock algorithms to histopathology data collected in two widely used mice strains. Future studies and replications in the same strains and/or in other mouse strains will disentangle similarities and differences across various strains. Quantifying individual Clock levels can be used to more precisely understand mechanisms of aging [41-43] and assess the rate of aging using cross-species translational tools to disentangle age-related similarities and differences and assess organ-, strain- and sex-specific effects of aging intervention studies. Using Bayesian inference allows us to predict such Clocks in established as well as new models and updates can be made when new information at physiological or pathological data become available.

Declarations

Availability of data and materials: Not applicable.

Financial support and sponsorship: Supported by NIH grants NIA-B K01AG059898 (PI, Shabnam Salimi), R24 AG047115, R56 AG058543, and R01 AG057381 (PI, Warren Ladiges), and P30 AG067000 (PI, Kaberlein).

Conflicts of interest: Warren Ladiges is a member of the Editorial Board of *Aging Pathobiology and Therapeutics.* All authors declare no conflict of interest and were not involved in the journal's review or desicions related to this manuscript.

Ethical approval and consent to participate: Not applicable.

References

1. Fabbri E, Zoli M, Gonzalez-Freire M, et al. Aging and multimorbidity: new tasks, priorities, and frontiers for integrated gerontological and clinical research. Journal of the American Medical Directors Association, 2015, 16(8): 640-647.
2. Salive M E. Multimorbidity in older adults. Epidemiologic Reviews, 2013, 35(1): 75-83.
3. Salive M E, Suls J, Farhat T, et al. National Institutes of Health Advancing Multimorbidity Research. Medical Care, 2021, 59(7): 622-624.
4. Ferrucci L, Gonzalez-Freire M, Fabbri E, et al. Measuring biological aging in humans: A quest. Aging Cell, 2020, 19(2): e13080.
5. Ladiges W. The emerging role of geropathology in preclinical aging studies. Pathobiology of Aging & Age-related Diseases, 2017, 7(1): 1304005.
6. Olstad K J, Imai D M, Keesler R I, et al. Development of a Geropathology Grading Platform for nonhuman primates. Aging Pathobiology and Therapeutics, 2020, 2(1): 16.
7. Rockwood K, Blodgett J M, Theou O, et al. A frailty index based on deficit accumulation quantifies mortality risk in humans and in mice. Scientific Reports, 2017, 7(1): 1-10.
8. Whitehead J C, Hildebrand B A, Sun M, et al. A clinical frailty index in aging mice: comparisons with frailty index data in humans. Journals of Gerontology Series A: Biomedical Sciences and Medical Sciences, 2014, 69(6): 621-632.
9. Feridooni H A, Kane A E, Ayaz O, et al. The impact of age and frailty on ventricular structure and function in C57BL/6J mice. The Journal of Physiology, 2017, 595(12): 3721-3742.
10. Snyder J M, Snider T A, Ciol M A, et al. Validation of a geropathology grading system for aging mouse studies. GeroScience, 2019, 41(4): 455-465.
11. Ladiges W. Pathology assessment is necessary to validate translational endpoints in preclinical aging studies. Pathobiology of Aging & Age-related Diseases, 2016, 6: 31478.
12. Schultz M B, Kane A E, Mitchell S J, et al. Age and life expectancy clocks based on machine learning analysis of mouse frailty. Nature Communications, 2020, 11(1): 1-12.
13. Richardson A, Fischer K E, Speakman J R, et al. Measures of healthspan as indices of aging in mice—a recommendation. Journals of Gerontology Series A: Biomedical Sciences and Medical Sciences, 2016, 71(4): 427-430.

14. Schriner S E, Linford N J, Martin G M, et al. Extension of murine life span by overexpression of catalase targeted to mitochondria. Science, 2005, 308(5730): 1909-1911.
15. Niedernhofer L J, Kirkland J L, Ladiges W. Molecular pathology endpoints useful for aging studies. Ageing Research Reviews, 2017, 35: 241-249.
16. Salimi S, Vehtari A, Salive M, et al. Body clock: Matching personalized multimorbidity and fast aging using information entropy. MedRxiv, 2021,
17. Pena A, Michelsen M M, Mygind N D, et al. Coronary microvascular dysfunction is associated with cardiac time intervals in women with angina and no obstructive coronary artery disease: An iPOWER substudy. Echocardiography, 2019, 36(6): 1110-1117.
18. Dai D F, Santana L F, Vermulst M, et al. Overexpression of catalase targeted to mitochondria attenuates murine cardiac aging. Circulation, 2009, 119(21): 2789-2797.
19. Ge X, Cho A, Ciol M A, et al. Grip strength is potentially an early indicator of age-related decline in mice. Pathobiology of Aging & Age-related Diseases, 2016, 6(1): 32981.
20. Ge X, Ciol M A, Pettan-Brewer C, et al. Self-motivated and stress-response performance assays in mice are age-dependent. Experimental Gerontology, 2017, 91: 1-4.
21. Goh J, Ladiges W. Voluntary wheel running in mice. Current Protocols in Mouse Biology, 2015, 5(4): 283-290.
22. Seibenhener M L, Wooten M C. Use of the open field maze to measure locomotor and anxiety-like behavior in mice. Journal of Visualized Experiments, 2015, 96: e52434.
23. Magnusson K R. Aging of glutamate receptors: correlations between binding and spatial memory performance in mice. Mechanisms of Ageing and Development, 1998, 104(3): 227-248.
24. Pettan-Brewer C, Touch D V, Wiley J C, et al. A novel radial water tread maze tracks age-related cognitive decline in mice. Pathobiology of Aging & Age-related Diseases, 2013, 3(1): 20679.
25. Wolf N, Pendergrass W, Singh N, et al. Radiation cataracts: mechanisms involved in their long delayed occurrence but then rapid progression. Molecular Vision, 2008, 14: 274.
26. Bürkner P C, Vuorre M. Ordinal regression models in psychology: A tutorial. Advances in Methods and Practices in Psychological Science, 2019, 2(1): 77-101.
27. Bürkner P C, Charpentier E. Modelling monotonic effects of ordinal predictors in Bayesian regression models. British Journal of Mathematical and Statistical Psychology, 2020, 73(3): 420-451.
28. Gelman A, Carlin J B, Stern H S, et al. Bayesian Data Analysis Chapman & Hall. CRC Texts in Statistical Science, 2004.
29. Vehtari A, Gelman A, Gabry J, Practical Bayesian model evaluation using leave-one-out cross-validation and WAIC. Statistics and Computing, 2017, 27(5): 1413-1432.
30. Bürkner P C. Advanced Bayesian multilevel modeling with the R package brms. The R Journal, 2018, 10(1): 395–411
31. Vehtari A, Simpson D, Gelman A, et al. Pareto smoothed importance sampling. 2015, 1507: 02646.
32. Gelman A, Goodrich B, Gabry J, et al. R-squared for Bayesian regression models. The American Statistician, 2019.
33. Vehtari A, Gelman A, Simpson D, et al. Rank-normalization, folding, and localization:An improved R-hat for assessing convergence of MCMC. Bayesian Analysis, 2020, 1- 28.
34. Yao Y, Vehtari A, Simpson D, et al. Using stacking to average Bayesian predictive distributions (with discussion). Bayesian Analysis, 2018, 13(3): 917-1007.
35. Unlu O, Levitan E B, Reshetnyak E, et al. Polypharmacy in older adults hospitalized for heart failure. Circulation: Heart Failure, 2020, 13(11): e006977.
36. Biering-Sørensen T, Mogelvang R, Schnohr P, et al. Cardiac time intervals measured by tissue Doppler imaging M-mode: association with hypertension, left ventricular geometry, and future ischemic cardiovascular diseases. Journal of the American Heart Association, 2016, 5(1): e002687.
37. Biering-Sørensen T, Mogelvang R, Jensen J S. Prognostic value of cardiac time intervals measured by tissue Doppler imaging M-mode in the general population. Heart, 2015, 101(12): 954-960.
38. Schumacher A, Khojeini E, Larson D. ECHO parameters of diastolic dysfunction. Perfusion, 2008, 23(5): 291-296.
39. Duggal N A, Niemiro G, Harridge S D R, et al. Can physical activity ameliorate immunosenescence and thereby reduce age-related multi-morbidity? Nature Reviews Immunology, 2019, 19(9): 563-572.
40. Klug J, Christensen S, Imai D M, et al. The geropathology of organ-specific aging. Journal of Translational Science, 2021.
41. Melis J P, Jonker M J, Vijg J, et al. Aging on a different scale–chronological versus pathology-related aging. Aging, 2013, 5(10): 782.
42. Salimi S. Perspective on multimorbidity and genetic theories of aging. Preprint, 2021.
43. Vijg J. From DNA damage to mutations: all roads lead to aging. Ageing Research Reviews, 2021, 101316.

Cite this article as: Salimi S, Pettan-Brewer C, Ladiges W. PathoClock and PhysioClock in mice recapitulate human multimorbidity and heterogeneous aging[J]. Aging Pathobiology and Therapeutics, 2021, 3(4): 107-126.